Nikapitiya *et al. Micro and Nano Syst Lett (2017) 5:24*
DOI 10.1186/s40486-017-0058-6

Micro and Nano Systems Letters

LETTER Open Access

Accurate, consistent, and fast droplet splitting and dispensing in electrowetting on dielectric digital microfluidics

N. Y. Jagath B. Nikapitiya, Mun Mun Nahar and Hyejin Moon*

Abstract

This letter reports two novel electrode design considerations to satisfy two very important aspects of EWOD operation—(1) Highly *consistent* volume of generated droplets and (2) Highly improved *accuracy* in the generated droplet volume. Considering the design principles investigated two novel designs were proposed; L-junction electrode design to offer high throughput droplet generation and Y-junction electrode design to split a droplet very fast while maintaining equal volume of each part. Devices of novel designs were fabricated and tested, and the results are compared with those of conventional approach. It is demonstrated that inaccuracy and inconsistency of droplet volume dispensed in the device with novel electrode designs are as low as 0.17 and 0.10%, respectively, while those of conventional approach are 25 and 0.76%, respectively. The dispensing frequency is enhanced from 4 to 9 Hz by using the novel design.

Keywords: Electrowetting on dielectric, Digital microfluidics, Dispensing, Splitting, Volume inaccuracy, Volume inconsistency, Dispensing frequency

Background

Electrowetting on dielectric (EWOD) digital microfluidics is a promising method of droplet manipulation that controls each droplet individually by an applying external electric field to the designated electrodes [1–3]. Since creating discrete droplets and pumping of liquids are done by surface tension alone, EWOD digital microfluidics does not require intricate systems such as channels, pumps and valves to drive and regulate flows [4, 5]. In addition, direct manipulation of discrete droplets enables fabrication and operation of highly automated microfluidics systems with more flexibility and higher efficiency [6–12]. Due to these unique advantages, EWOD digital microfluidics has been used for tremendous applications such as medical [13–19], display [20, 21], optics [22, 23], and cooling [24, 25]. In addition, there are many recent EWOD studies on engineering applications such as optofluidics and solar energy [26, 27]. In most of these applications, flow rate, concentration, and energy transfer rate are totally dependent on the volume of a unit droplet and their arrival frequency to a designated area. Therefore, accuracy and consistency of the volume of a unit droplet and its dispensing frequency are extremely important.

Inaccuracy in volume of the dispensed droplet is defined by the difference between the actual dispensed volume and the predicted (e.g. target) volume (volume subtended by the droplet dispensing electrode) divided by the predicted volume. Usually, volume inaccuracy of less than ±5% is sufficient for most of the biomedical applications [28]. Although there are very few reports regarding volume accuracy in droplet dispensing, it is well known that the actual dispensed volume is usually larger than the predicted volume [29] due to the extra amount of liquid added by liquid tail.

On the other hand, inconsistency in volume of the dispensed droplet is defined by the fraction of standard deviation associated with a set of dispensed volumes to their mean value. It was reported that the volume inconsistency must be below 10%, and preferably below 5% for drug discovery applications, while it needs to be

*Correspondence: hyejin.moon@uta.edu
Mechanical and Aerospace Engineering Department, The University of Texas at Arlington, Arlington, TX 76019, USA

maintained within 2% for microdialysis applications [28, 30]. Many previous literatures concerned poor consistency of EWOD devices [31–33] and suggested using of capacitance metering with feedback control and/or external pressure sources. However, these methods make device assembly complicate and bulky.

Therefore, this study presents a very simple method to improve volume accuracy and consistency as well as frequency in droplet dispensing in EWOD microfluidics by solely focusing on geometry of electrodes in a device. Firstly, design principles that affect the dispensed volume were set. Secondly, model designs that meet the principles were proposed, fabricated, tested and compared with the conventional approach.

Device design principles

In the conventional approach, a reservoir holds larger amount of liquid from which smaller unit droplets on demand can be generated. Figure 1a shows a representative electrodes design. Electrode E_3 is activated first and is filled with liquid. Electrodes E_2 and E_1 are next turned on to pull liquid from E_3. As soon as the surface over E_1 is completely wet, E_3 is turned on and E_2 is turned off simultaneously. At this stage, wetting forces from both E_1 and E_3 from opposite directions act in parallel to the direction of the liquid motion, while de-wetting forces on E_2 act perpendicularly on the liquid bridge formed between two active electrodes. As a result, a 'neck' is formed on E_2 which continuously keeps shrinking until two de-wetting menisci meet with each other and tear the liquid into two parts on two sides. For dispensing, it is intended that a generated droplet would completely wet the area over E_1 and pinch-off would happen very near to the right edge of E_1. To make this happen, first of all, duration of voltage application on generating electrode (E_1) should be long enough so that the liquid has enough time to completely wet the surface over E_1. At the same time, the Laplace pressure drop, ΔP at the neck should

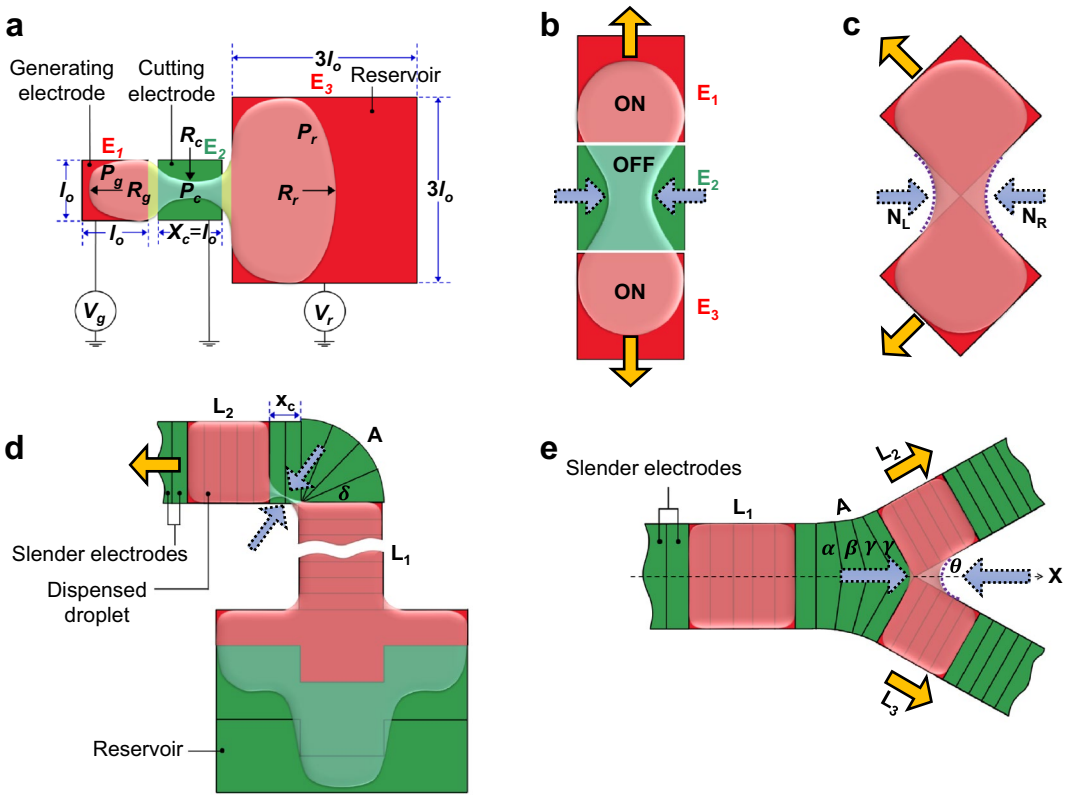

Fig. 1 **a** Droplet generation in conventional reservoir. Here, l_o is the representative electrode dimension and x_c is the cutting length. P and R denote the pressure and radius of curvatures respectively with the subscripts referring to particular electrodes. **b** Droplet splitting using conventional approach. *Yellow* (*solid*) and *blue* (*dotted*) *arrows* indicate electrowetting and de-wetting forces respectively. **c** Ideal droplet splitting concept with the *yellow* and *blue arrows* as representative of electrowetting and de-wetting forces. N_L and N_R denote the *left* and *right* meniscus at the junction between the *diamond shaped* electrodes. **d** Droplet generation in L-junction with 'L_1','L_2' being the linear segments whereas 'A' as the angled section. δ is the angle of each slender electrodes in section 'A'. **e** Droplet cutting in Y-junction. Linear sections L_1, L_2 and L_3 are composed of straight slender electrodes whereas arc section A is composed of slender electrodes with angles α, β and γ. The *dashed line*, *X* denotes the *horizontal axis* towards the initial droplet motion

reach a critical value, ΔP_{cr} adjacent to the right edge of electrode, E_1. However, in the most of the time, there is the mismatch between velocities of leading meniscus and de-wetting meniscus, therefore the neck forms much later than the liquid finger front reaches to the electrode. A tail is formed on the cutting electrode (E_2), thus after pinch-off, droplet volume is typically larger than the intended volume. If the cutting length x_c is shorter, the tail also becomes shorter and the amount of dispensed volume deviates less from the expected volume. However, there exists a minimum cutting length, $(x_c)_{min}$ below which droplet generation ceases [Additional file 4], which makes it impossible to completely remove the additional volume to a dispensed droplet with the conventional approach.

Another issue with conventional approach is the inconsistency in the volume of dispensed droplets for a given set of parameters. It has been shown by our previous study that, for the same cutting length, x_c, the location of the neck can differ during multiple generations due to difference in the reservoir liquid volume [34]. It mainly happens when after repeated dispensing, the reservoir liquid gets depleted and the curvature of the liquid interface at the left reservoir boundary is changed thus leading to change in ΔP_{cr} at the neck as well as the location of the neck.

Keeping the above discussion in mind, to maintain volume accuracy and consistency of droplet generation, it is deduced that the device should meet two criteria respectively:

(1) There should be no tail, if not, the tail should be minimized and; (2) the neck should always form at the same position.

To envision one technique to satisfy the above two conditions, one can start from investigating splitting scenarios of a droplet. In the conventional way of splitting shown in Fig. 1b, a parent droplet is pulled by electrowetting forces exerted on two opposite sides of the droplet while the middle portion experiences de-wetting forces. In the middle portion, two menisci move toward each other (i.e., form a neck) and then split the droplet into two parts when they meet. This technique will split a droplet into two equal volumes as long as the splitting is symmetric. However, in typical dispensing scenario, splitting is not symmetric because the reservoir electrode should be much larger than generating electrode, hence, it easily violates two criteria stated above. Now we can consider an alternative splitting scenario (Fig. 1c) to avoid a long and passive neck formation. As shown in Fig. 1c, if a parent droplet experiences electrowetting forces by two electrodes arranged diagonally, the droplet will conform to the electrodes shape to have two diamond portions connected with a very tiny liquid bridge. This tiny liquid bridge is easy to break with small perturbation and the parent droplet readily splits into two equal daughter droplets. This new scenario would meet two criteria because there is no tail involved before breakup and the pinch-off of droplet will happen at the point shared by two diagonal electrodes.

This ideal splitting method is introduced in our proposed reservoir design as shown in Fig. 1d. First a column L_1 is filled by liquid pulled from the filling section of the reservoir. Next, liquid is further transported across arc section A and placed on second linear section L_2. Both L_1, L_2 are divided into slender (instead of square) electrode segments. Arc A is also composed of four sectors. All of these segments can be individually addressed. Note that, A is not filled with liquid and only used to carry liquid to L_2. Since L_1 and L_2 create a right angle, liquid on those two sections touch each other diagonally just before pinch-off, which is similar to that in Fig. 1c. Later, liquid column L_1 is held in place by activating all of the electrodes while pulling force is applied on the liquid on L_2 from left. Without generating any elongated tail, pinch-off happens very close to the junction point of L_1 and L_2. Like the ideal splitting scheme already discussed and shown in Fig. 1c, the tail formed after pinch-off is expected to be very tiny in this case and therefore dispensed volume should be very accurate. Also, because the liquid column L_1 is fixed, the volume in the filling section is not likely to affect the meniscus formation in the neck and thus will not affect location of the pinch-off point. The use of the slender electrodes in L_1 and L_2 serves two additional purposes: first, it controls the deformation thus making sure that the necking will happen very close to the L_1–L_2 junction and second, it speeds up the process by enhancing the transport velocity of liquid [35]. Due to the latter advantage, this reservoir design would also give higher droplet generating rate as well.

For increasing the generating rate further, a Y-junction splitting unit is proposed which can serve as an additional splitting unit alongside the L-junction reservoir which can be used to split the droplets further after they have been generated in L-junction reservoir to double the generating rate or it can act as a stand-alone droplet splitter when symmetric and faster droplet splitting is needed. In a Y-junction splitter, a unit droplet is first transported via an array of slender electrodes and placed on linear section 'L_1'. It is followed by a second section 'A' which is composed of a set of angular electrodes. Section 'A' is then branched into two linear sections, 'L_2' and 'L_3' which are apart from each other at an angle of 2θ. As shown in Fig. 1e, faded red areas show the regions filled with liquid just before the pinch off. When electrowetting force is applied on them in the direction indicated by yellow arrows, the neck which is nothing but the thin liquid

bridge between the two sections (L_2 and L_3), moves to the right along x-axis. Gradually, the radii of curvature of menisci N_L and N_R would keep decreasing while decreasing the corresponding Laplace pressure drops until the breakup happens. This is a slightly modified version of the ideal splitting technique described earlier. This splitting mechanism would ensure equal splitting, as well as consistency in the location of the pinch-off point. Also, use of the slender electrodes makes the splitting much faster [35] than the conventional splitting technique as described in Fig. 1b.

Methods

Device fabrication, data collection, and data analysis

All EWOD devices were fabricated in Nanofab in University of Texas at Arlington. Indium tin oxide (ITO) electrodes (~100 nm) were patterned by wet etching of ITO after photolithography on an ITO coated glass substrate. Dielectric layer (SU-8, 5 μm) and hydrophobic layer (Teflon, 300 nm) were spin-coated and oven baked. The details of the fabrication steps can be found in Additional file 5. The droplet motion was recorded using a high-speed camera (Model: Miro M310, Vision Research; frame rate: 1000 fps; resolution: 512 × 480). To measure the volume of dispensed droplets, the footprint area of a droplet was determined by image processing using ImageJ software. Since droplets are placed between top and bottom plates of which gap was carefully controlled to be parallel to each other and to have a known spacer gap which serves as the height of a droplet, the volume of droplet was simply estimated by multiplying the footprint area and the spacer gap.

Test methods

Average volume inaccuracy and inconsistency of droplet dispensing and splitting from the conventional, L and Y-junction devices have been investigated. From conventional reservoir, ten droplets have been sequentially dispensed, and normalized volume of the dispensed droplet has been calculated. In L and Y-junction devices, 10 sequentially generated droplets have been tested. For comparison purpose, droplet splitting using two conventional schemes has been performed. The spacer gap between the top plate and the bottom plate of the EWOD device was 100 μm. The area of the generating electrode was 2×2 mm^2 for the conventional reservoir. For the slender electrodes in L and Y-junction devices, area was $.4 \times 2$ mm^2. Properties of the liquid (DI water) in the current study are given in the Additional file 4: Table A1. Note that a typical dispensing process fulfills three fundamental stages (filling stage, cutting stage and relocating stage). In the filling stage, reservoir liquid flows towards the cutting and generating electrodes (E_2 and E_1) until the two electrodes are filled with liquid. In the cutting stage, the two de-wetting menisci move towards each other in opposite directions until the liquid neck pinches off creating a small droplet on the generating electrode (E_1). In the relocating stage, the dispensed droplet on the generating electrode is relocated by EWOD for further actions. Note that the filling stage should be allowed sufficient filling time to reach the steady state. However, it is difficult to determine the completion of the filling stage by simply observing the motion of the liquid interface. Therefore, a sufficiently longer filling time is chosen (1000 ms).

Results and discussion

Droplet generation

Details of droplet generating process using conventional process have been discussed in our previous work [34]. Figure 2 shows the snapshots of the main steps of droplet pinch-off in L-junction. Liquid is filled up to the first electrode in linear segment L_2 (Fig. 2a). Next, the first electrode on the arc A is turned off and the second electrode in L_2 is turned on (Fig. 2b). In the next three steps (Fig. 2c–e), consecutive electrodes in arc A are turned off one at a time while one additional electrode at the left on L_2 is turned on so that 5 consecutive electrodes are progressively activated in order to achieve the arrangement as shown in Fig. 2e. In the next two steps (Fig. 2f, g), electrodes on L_2 are activated using 4–5 scheme [35] and the neck between L_2 and L_1 are slightly stretched until it breaks off.

If we closely observe the Fig. 2b–e, while the liquid flow preceeds from the first linear electrode segment (L_1) into the second linear electrode segment (L_2), during each step of transition, the angle which confines the top de-wetting meniscus becomes larger and the radius of curvature is increased. As a result, the Laplace pressure drop keeps increasing which forces the top de-wetting meniscus to move toward the inner side of the arc A. Throughout this whole period of time, bottom meniscus is fixed over the right angle and the width of the neck is reduced. The main factor affecting the neck formation is the turn of right angle which facilitates diagonal contact arrangement of the splitting volumes.

Figure 3 summarizes the results from the experiments using conventional and L-junction reservoirs. The large error bar associated with the conventional reservoir indicates that a generated droplet would have almost 30% higher volume than intended volume leading to a 25% inaccuracy, which is much higher than the acceptable limit in some applications [28]. The conventional

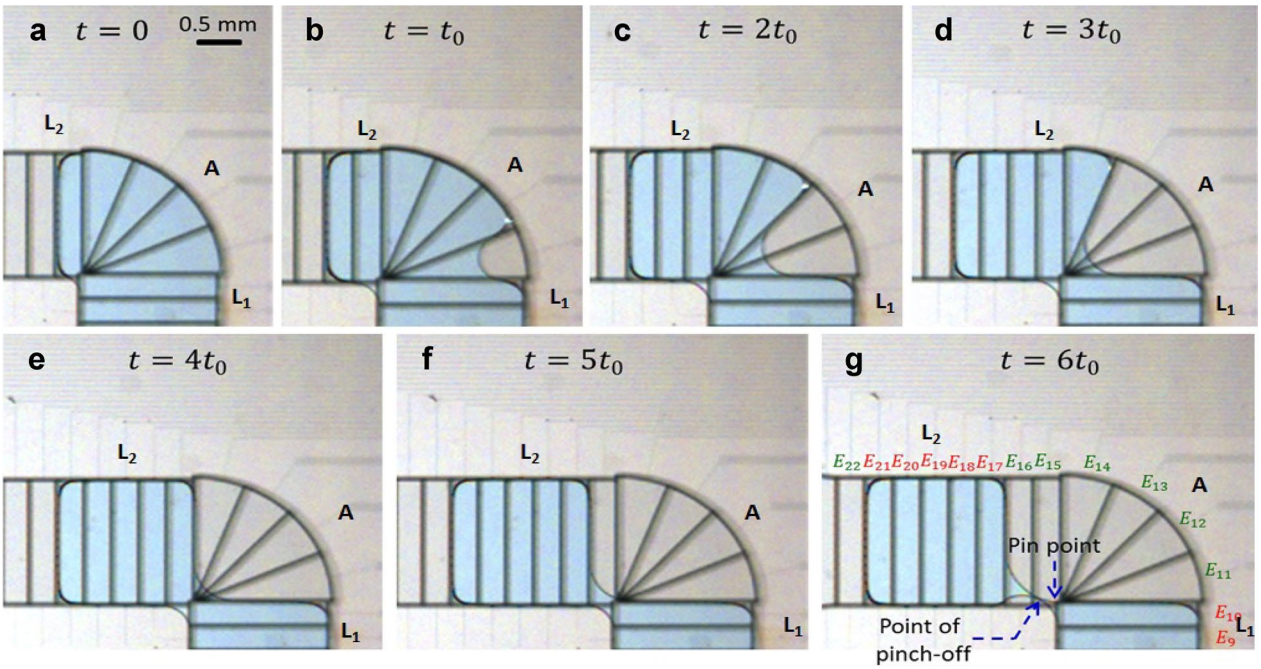

Fig. 2 Steps of droplet dispensing process in L-junction device. t_0 is the time interval between electrodes turned on and off. **a** Liquid meniscus entered section L2, **b**–**e** A liquid segment is being developed by sequentially turning on electrodes in section L2 while sequentially turning off electrodes in section A. **f** The liquid segment is shaped after all the meniscus entered to section L2. **g** A droplet is formed (e.g. dispensed) when the segment keeps moving in L2 so that the tail of the segment pinches off

reservoir also has less efficiency in reproducing the droplets with the same volume which is reflected by the slightly larger inconsistency percentage compared to L-junction (0.766% vs. 0.104%). The better accuracy and consistency in L-junction devices can be attributed to its ability to create the pinch-off point at a fixed location and to reduce the tail length before pinch-off as discussed earlier. On the other hand, in conventional reservoirs, during the liquid filling stage, the intercept length at the left edge (as shown in Fig. 1a) may vary depending on the volume present in that area. Clearly, it will affect the curvature at the neck and also the critical Laplace pressure ΔP_{cr} [34]. This variation will lead to the variation in the location of the pinch-off point as well as the generated volume. Apart from having the advantages of better volume accuracy and consistency, L-junction devices can generate droplets much faster compared to the conventional reservoirs. The frequency of droplet generation is also increased significantly to 9–18 (Hz) depending on the device and experimental conditions which is almost 2–4 times of the generating rate in conventional reservoir.

Droplet splitting

Splitting performance of a Y-junction device was tested. Snapshots in Fig. 4 show the splitting of a droplet into two equal-volume droplets in Y-junction device. When the droplet starts entering the two angled branches, the right de-wetting meniscus remains confined within the 2θ angle where the angle (θ) is 30 degrees (Fig. 4a). At the same time, radius of curvature of the left de-wetting meniscus keeps decreasing (Fig. 4b–e) until it becomes constant (from Fig. 4e through Fig. 4h). The left de-wetting meniscus experiences gradual decrease in radius of curvature and corresponding decrease in Laplace pressure until it progresses into the angled section (Fig. 4g). Since the right de-wetting meniscus remains fixed and only left de-wetting meniscus moves to the right, pinch-off happens at the right side of the pin-point.

Figure 4i and j are representative of conventional splitting scenarios. In scheme I, the initial droplet sits on two adjacent square electrodes. Next, the two other electrodes on each side of the droplet are turned on while turning off the electrodes underneath the droplet. The droplet is pulled by opposing electrowetting forces and a

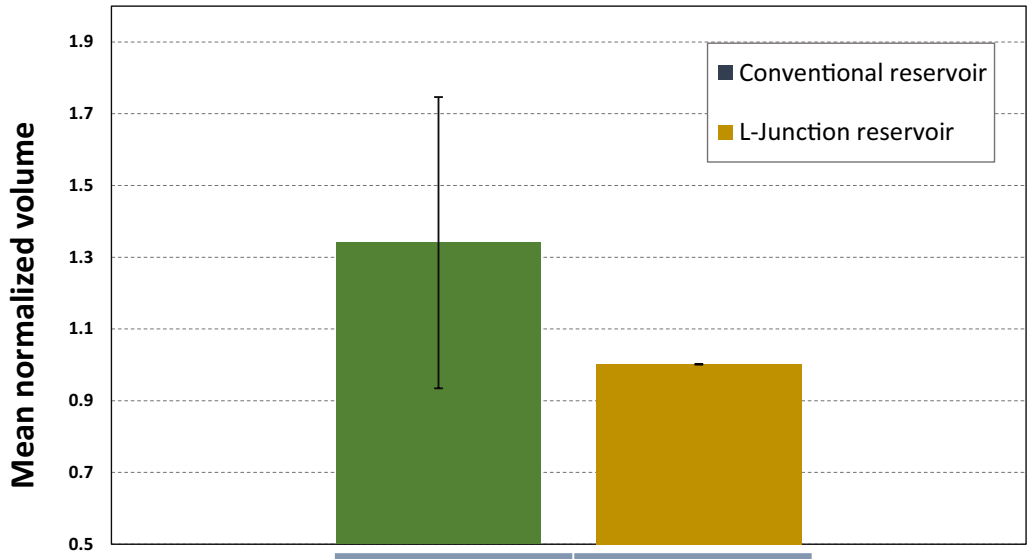

	Conventional reservoir	L-Junction reservoir
Mean	1.34044	1.0017
STD	0.01027	0.0010
Inaccuracy (%)	25.3978	0.1702
Inconsistency (%)	0.76642	0.1042
Dispensing time (ms)	230 ms	55-110 ms

Fig. 3 Mean normalized volume of generated droplets from conventional reservoir and L-junction reservoir. The *error bars* correspond to the standard deviations. Tabulated values are the summary of tests performed on 10 droplets for both cases

neck is formed in the middle. After a certain amount of time has passed, neck narrows down further thus breaking the droplet into two parts. The two droplets now completely move over to the two activated neighboring electrodes. Scheme II is slightly different from scheme I. Splitting is initiated when the middle electrode is turned off, while the third electrode on right is turned on. This way, the left portion of the droplet stays on the activated electrode on the left side, but the other portion starts to move towards the newly activated electrode on the right. A neck is formed on the deactivated electrode at the middle and later pinch-off happens at the pinch-off location. In both of these cases, the neck experiences instability and pinch off-location is not fixed. As a result, the two resulting droplets are not equal in volume and there exists considerable inconsistency in the volume as well.

Figure 5 shows the results from the splitting tests. The columns represent the mean normalized volume of the

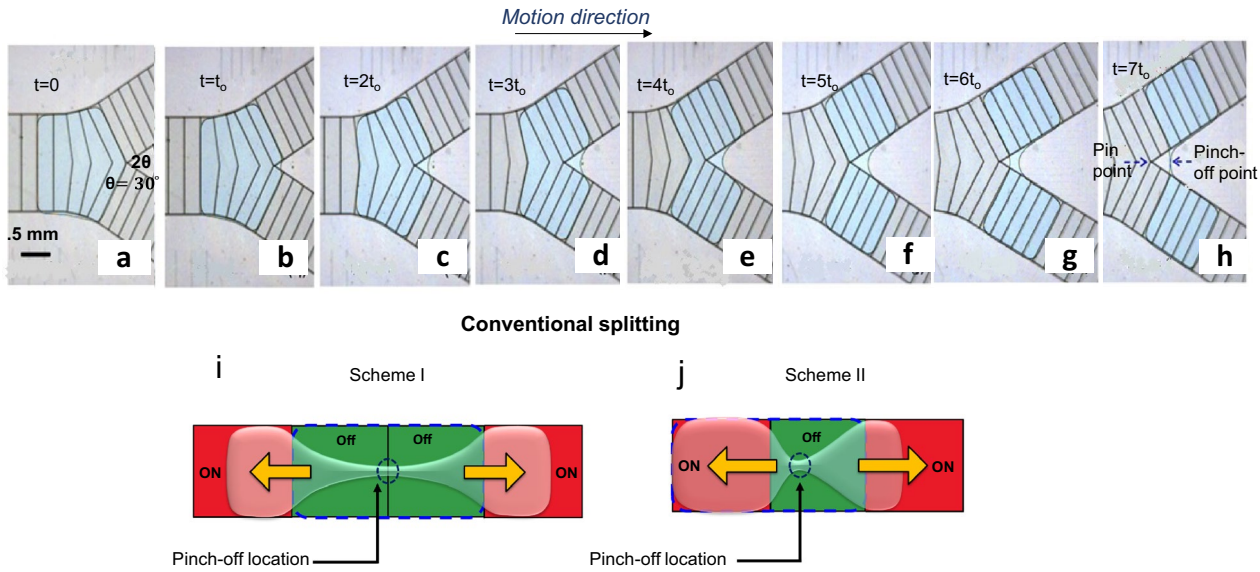

Fig. 4 **a**–**h** Steps of the process of splitting a droplet by Y-junction with switching time (t0). The location of pinch-off occurs on the *right* from the pin-point. 2θ is the angle between two branches of Y-junction. **i**–**j** Droplet splitting in conventional device with scheme I and II respectively. The *yellow arrows* show fluid motion during splitting. *Blue dashed line* is the initial droplet profile

splitted droplets and the error bars correspond to the standard deviations. As we can see, a large amount of inaccuracy (more than 4%) is associated with scheme I. Also, in terms of inconsistency, scheme II is again slightly better than scheme I. This is because scheme II has comparatively better control on the pinch-off point since at the beginning of pinch-off, a large part of the droplet is already on the destined electrode and only the other half moves on the opposite direction. Compared to these two schemes, Y-junction can provide much better splitting in terms of accuracy and consistency. The inaccuracy is less than 0.1% and the inconsistency is only 0.02%. As discussed earlier, the success of Y-junction splitting is related to the fact that, like the L-junction device, it can manage to reduce the tail length significantly and also can restrict the pinch-off point to occur at a fixed position. It should be also noted that, both of the schemes I and II fail to result in equal splitting. It is intrinsic to scheme II and is obvious. In scheme II, since the left portion is already filled with liquid, whenever the tail forms somewhere at the middle electrode before the pinch off-point, it adds up to the droplet generated on the left making the droplet on the right to be slightly smaller in volume. In general, other factors like uneven channel gap, irregular surface properties can influence any of the droplets to be larger or smaller than the other. However, for the Y-junction, the droplets have almost equal volume after splitting. Another big advantage is the enhanced rate of droplet splitting in Y-junction device. Compared to the 135 ms in conventional schemes, Y-junction device is capable of splitting droplets in just 35–70 ms depending on the device and experimental conditions, which is almost 2–4 times faster than the conventional method.

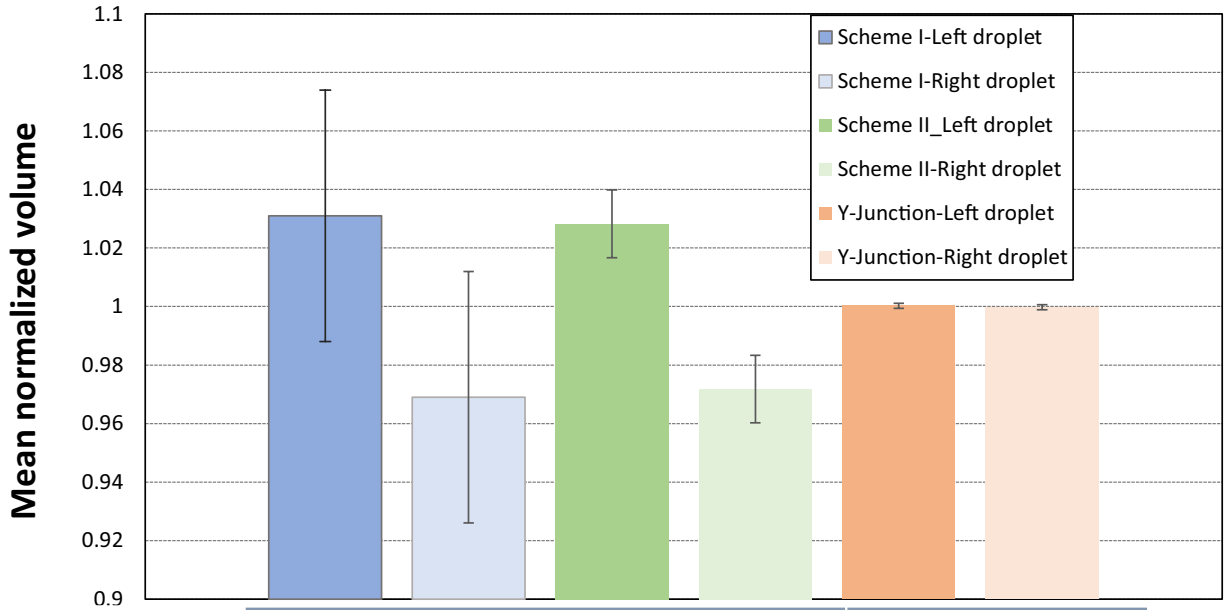

	Conventional splitting				Splitting in Y – Junction	
	Scheme I		Scheme II			
	Left droplet	Right droplet	Left droplet	Right droplet	Left droplet	Right droplet
Mean	1.031	0.969	1.0282	0.9718	1.000245	0.99970
STD	0.043	0.043	0.0116	0.0116	0.000854	0.00085
Inaccuracy (%)	4.167	4.433	1.1248	1.1901	0.085418	0.08546
Inconsistency (%)	3.005	3.199	2.7420	2.9010	0.024400	0.02450
Splitting time (ms)	135				35-70	

Fig. 5 Mean normalized volume of droplets after splitting using conventional method with two different schemes and using Y-junction. The *error bars* correspond to the standard deviations. Tabulated values are the summary of tests performed on 10 droplets for all cases

Conclusion

We have proposed and demonstrated a novel reservoir design to achieve two important criteria in a EWOD lab-on-a chip devices: a certain percentage of volume accuracy and consistency which are required in many biological applications. Compared to conventional reservoir, our proposed L-junction reservoir is 99% more accurate in dispensing a droplet with desired volume. Consistency is also improved by almost 87%. Almost same accuracy and consistency have been achieved by using Y-junction device. In terms of generating rate, L-junction can give 2–4 times increase and if Y-junction is added, it is possible to gain 4–8 times higher frequency in droplet generation.

Additional files

Additional file 1. Video of droplet dispensing in a conventional design of EWOD device.

Additional file 2. Video of droplet dispensing by L-junction followed by droplet splitting by Y-junction device.

Additional file 3. Video of droplet splitting by Y-junction device.

Additional file 4. Analysis to show the existence of minium cutting length (x_c).

Additional file 5. Detail description of EWOD device fabrication.

Authors' contributions

JN conceived the first designs of device. JN and MMN performed the experiments, analyzed the data and wrote the manuscript. HM supervised the research and reviewed the manuscript. All authors read and approved the final manuscript.

Competing interests

The authors declare that they have no competing interests.

Availability of data and materials

The datasets supporting the conclusions of this article are included within the article and its Additional files, Fig. 1: various droplet dispensing methods; Fig. 2: steps of the process of dispensing a droplet by L-junction; Fig. 3: normalized dispensed volume in conventional and L-junction reservoir; Fig. 4: steps of the process of splitting a droplet by Y-junction; Fig. 5: normalized volume of droplets after splitting by conventional approach and in Y-junction; Additional file 1: Video S1: experimental video for dispensing a droplet from conventional reservoir; Additional file 2: Video S2: experimental video for splitting a droplet from L-junction electrode design. Additional file 3: Video S3: experimental video for splitting a droplet from Y-junction electrode design; Additional file 4: derivations of the critical conditions for droplet pinch-off. Additional file 5: details of device fabrication.

Funding

This study was partially supported by the Defense Advanced Research Projects Agency/Microsystems Technology Office (DARPA/MTO) (Grant No. W31P4Q-11-1-0012) and National Science Foundation (NSF) (Grant No. 1254602).

Publisher's Note

Received: 28 February 2017 Accepted: 6 June 2017
Published online: 16 June 2017

References

1. Fair RB (2007) Digital microfluidics: is a true lab-on-a-chip possible? J Microfluid Nanofluid 3(3):245–281. doi:10.1007/s10404-007-0161-8
2. Teh SY, Lin R, Hung LH, Lee AP (2008) Droplet microfluidics. Lab Chip 8(2):198–220. doi:10.1039/B715524G
3. Choi K, Ng AHC, Fobel R, Wheeler AR (2012) Digital microfluidics. Annu Rev Anal Chem 5(1):413–440. doi:10.1146/annurev-anchem-062011-143028
4. Bahadur VA, Garimella SV (2006) An energy-based model for electrowetting-induced droplet actuation. J Micromech Microeng 16(8):1494–1503. doi:10.1088/0960-1317/16/8/009
5. Cooney CG, Chen CY, Emerling MR, Nadim A, Sterling JD (2006) Electrowetting droplet microfluidics on a single planar surface. J Microfluid Nanofluid 2(5):435–446. doi:10.1007/s10404-006-0085-8
6. Zeng J, Korsmeyer T (2004) Principles of droplet electrohydrodynamics for lab-on-a-chip. Lab Chip 4(4):265–277. doi:10.1039/B403082F
7. Pollack MG, Fair RB, Shenderov AD (2000) Electrowetting-based actuation of liquid droplets for microfluidic applications. Appl Phys Lett 77(11):1725–1726. doi:10.1063/1.1308534
8. Baird E, Young P, Mohseni K (2006) Electrostatic force calculation for an EWOD-actuated droplet. J Microfluid Nanofluid 3(6):635–644. doi:10.1007/s10404-006-0147-y
9. Chiou PY, Park S-Y, Wu MC (2008) Continuous optoelectrowetting for picoliter droplet manipulation. Appl Phys Lett 93(2):221110. doi:10.1063/1.3039070
10. Park S-Y, Chiou P-Y (2011) Light-driven droplet manipulation technologies for lab-on-a-chip applications. Adv OptoElectron 909174:1–12. doi:10.1155/2011/909174
11. Jiang DY, Park S-Y (2016) Light-driven 3D droplet manipulation on flexible optoelectrowetting devices fabricated by a simple spin-coating method. Lab Chip 16:1831–1839. doi:10.1039/c6lc00293e
12. Park S-Y, Teitellb MA, Chiou EPY (2010) Single-sided continuous optoelectrowetting (SCOEW) for droplet manipulation with light patterns. Lab Chip 10(13):1655–1661. doi:10.1039/c001324b
13. Miller EM, Wheeler AR (2008) A digital microfluidic approach to homogeneous enzyme assays. Anal Chem 80(5):1614–1619. doi:10.1021/ac702269d
14. Sista R, Hua Z, Thwar P, Sudarsan A, Srinivasan V, Eckhardt A, Pollack M, Pamula V (2008) Development of a digital microfluidic platform for point of care testing. Lab Chip 8(12):2091–2104. doi:10.1039/B814922D
15. Chang YH, Lee GB, Huang FC, Chen YY, Lin JL (2006) Integrated polymerase chain reaction chips utilizing digital microfluidics. Biomed Microdevice 8(3):215–225. doi:10.1007/s10544-006-8171-y
16. Srinivasan V, Pamula VK, Fair RB (2004) An integrated digital microfluidic lab-on-a-chip for clinical diagnostics on human physiological fluids. Lab Chip 4(4):310–315. doi:10.1039/B403341H
17. Luk VN, Wheeler AR (2009) A digital microfluidic approach to proteomic sample processing. Anal Chem 81(11):4524–4530. doi:10.1021/ac900522a
18. Namgung B, Tan JKS, Wong PA, Park S-Y, Leo HL, Kim S (2016) Biomimetic precapillary flow patterns for enhancing blood plasma separation: a preliminary study. Sensors 16(9):1543–1553. doi:10.3390/s16091543
19. Shen H-H, Fan S-K, Kim C-J, Yao D-J (2014) EWOD microfluidic systems for biomedical applications. Microfluid Nanofluid 16(5):965–987. doi:10.1007/s10404-014-1386-y
20. Sureshkumar P, Bhattacharyya SS (2012) Display applications of electrowetting. J Adhes Sci Technol 26(12–17):1947–1963
21. Charipar KM, Charipar NA, Bellemare JV, Peak JE, Piqué A (2015) Electrowetting displays utilizing bistable, multi-color pixels via laser processing. J Disp Technol 11(2):175–182. doi:10.1109/JDT.2014.2364189
22. Clement CE, Park S-Y (2016) High-performance beam steering using electrowetting-driven liquid prism fabricated by a simple dip-coating method. Appl Phys Lett 108(19):191601. doi:10.1063/1.4949265
23. Clement CE, Thio SK, Park S-Y (2017) An optofluidic tunable Fresnel lens for spatial focal control based onelectrowetting-on-dielectric (EWOD). Sens Actuators B 240:909–915. doi:10.1016/j.snb.2016.08.125
24. Sung-Yong Park S-Y, Na YS (2017) Single-sided digital microfluidic (SDMF) Devices for effective coolant delivery and enhanced two-phase cooling. Micromachines 8(1):3. doi:10.3390/mi8010003
25. Paik PY, Pamula VK, Chakrabarty K (2008) Adaptive cooling of integrated circuits using digital microfluidics. IEEE Trans Very Large Scale Integr VLSI Syst 16(4):432–443. doi:10.1109/TVLSI.2007.915434
26. Cheng JT, Park S-Y, Chen C-L (2013) Optofluidic solar concentrators using electrowetting tracking: concept, design, and characterization. Sol Energy 89:152–161. doi:10.1016/j.solener.2012.12.018
27. Narasimhan V, Jiang DY, Park S-Y (2016) Design and optical analyses of an arrayed microfluidic tunable prism panel for enhancing solar energy collection. Appl Energy 162:450–459. doi:10.1016/j.apenergy.2015.10.051
28. Rose D (1999) Microdispensing technologies in drug discovery. Drug Discov Today 4(9):411–419. doi:10.1016/S1359-6446(99)01388-4
29. Wang W, Jones TB, Harding DR (2011) On-chip double emulsion droplet assembly using electrowetting-on-dielectric and dielctrophoresis. Fusion Sci Technol 59(1):240–249
30. Ren H, Fair RB, Pollack MG (2004) Automated on-chip droplet dispensing with volume control by electro-wetting actuation and

capacitance metering. Sens Actuators B 98(2–3):319–327. doi:10.1016/j.snb.2003.09.030
31. Cho SK, Moon H, Kim CJ (2003) Creating, transporting, cutting, and merging liquid droplets by electrowetting-based actuation for digital microfluidics circuits. J of Microelctromech Syst 12(1):70–80. doi:10.1109/JMEMS.2002.807467
32. Gong J, Kim CJ (2008) All-electronic droplet generation on-chip with real-time feedback control for EWOD digital microfluidic. Lab Chip 8(6):898–906. doi:10.1039/B717417A
33. Elvira KS, Leatherbarrow R, Edel J, deMello A (2012) Droplet dispensing in digital microfluidic devices: assessment of long-term reproducibility. Biomicrofluidics 6(2):22003–2200310. doi:10.1063/1.3693592
34. Guan Y, Tong AY, Nikapitiya NYJB, Moon H (2016) Numerical modeling of microscale droplet dispensing in parallel-plate electrowetting-on-dielectric (ewod) devices with various reservoir designs. Microfluid Nanofluid 20(2):39. doi:10.1007/s10404-016-1703-8
35. Nahar MM, Nikapitiya NYJB, Moon H (2016) Droplet velocity in an electrowetting on dielectric digital microfluidic device. Micromachines 7(4):71. doi:10.3390/mi704007